# INTRODUCTION

**Research object**

- Research on the 3-3-1$\beta$ model, a flipped 3-3-1 model.
- The LFV source of the flipped 3-3-1 model.
- Investigate analytical formulas of one-loop contributions to the amplitude of the decays $h \to Z\gamma, \gamma\gamma$ in the 3-3-1$\beta$, $h \to e_a e_b, e_b \to e_a \gamma$ in the flipped 3-3-1 model.
- Investigate the branching rate of the decays $h \to \mu\tau$, $h \to Z\gamma$.

**Research objects and scope of the study**

- The coupling of LFV, the coupling related to the decay $h \to Z\gamma$, Feynman diagram and amplitude corresponding to the proposed decay.
- Passarino-Veltman (PV) function corresponding to 2 of the decays $h \to Z\gamma$, $e_a e_b$.
- Numerical survey of the decays $h \to Z\gamma$ and $h \to \mu\tau$ in 2 proposed models.

**Research content**

- The flipped 3-3-1 model and 3-3-1$\beta$ model.
- The analytical formulas of the LFVHD in the flipped 3-3-1 model.
- Numerical survey and discuss on the decay $h \to \mu\tau$ in the flipped 3-3-1 model.
- Analytical formulas of the decays $h \to Z\gamma, \gamma\gamma$ in the 3-3-1$\beta$.
- Numerical survey and discuss of the decay $h \to Z\gamma, \gamma\gamma$ in the 3-3-1$\beta$.

**Research methods**

- Using Quantum Field Theory to build analytical formulas.
- Mathematica software for numerical calculation.

**Structure of thesis:**

**Chapter 1:** We present particle spectra, the physical states of the leptons and bosons, the mixing parameters in the two models flipped 3-3-1 and 3-3-1$\beta$. This is the basis for us to calculate the couplings and investigate the decay processes related to this thesis.

**Chapter 2:** In this chapter, we have calculated the couplings related to the LFVHD in the flipped 3-3-1 model, constructed analytical formulas to calculate the branching ratio (BR) of the decays $h \to e_a e_b,\ e_a \to e_b \gamma$.

**Chaper 3:** We have investigated LFV decays of the SM-like Higgs boson $h \to \mu\tau$ and charged lepton $e_a \to e_b\gamma$ in the flipped 3-3-1 model. Assuming that all new heavy particles are in the TeV scale, $BR(h \to \tau\mu, \tau e)$ and $BR(h \to \mu e)$ can reach the orders of $\mathcal{O}(10^{-3} - 10^{-4})$ and $\mathcal{O}(10^{-6})$, respectively. These values are very close to the recent lower bounds reported by experiments, and they should be considered for constraining the parameter space of the model if improved lower bounds on these decay rates are announced. The large BR of LFVHD still appear even with heavy $m_{Z'} \sim \mathcal{O}(10)$ TeV. On the other hand, the BR$(e_b \to e_a\gamma)$ always satisfies the current experimental constraints. Specifically, BR$(\tau \to \mu\gamma, e\gamma) \leq \mathcal{O}(10^{-14})$, which are much smaller than the planned sensitivities of upcoming experiments. In contrast, BR$(\mu \to e\gamma)$ can reach the order of $\mathcal{O}(10^{-15})$, rather close to the planned experimental sensitivity of $6 \times 10^{-14}$.

**Chapter 4:** In this chapter, we have determined the couplings of the decays $h \to Z\gamma, \gamma\gamma$ in the 3-3-1$\beta$. The analytical formulas for amplitudes, branching ratios, and signal strengths were also shown.

**Chapter 5:** The signals of new physics predicted by the 3-3-1 models from the neutral Higgs boson decays $h, h_3^0 \to \gamma\gamma, Z\gamma$ have been discussed. For the general case with arbiltrary $\beta$ we have derived that Br$(h \to \gamma\gamma, Z\gamma)$ do not depend on the $\beta$, they cannot be used to distinguish different models corresponding to particular $\beta$ values. The large deviations of the signal strengths $\delta\mu_{Z\gamma,\gamma\gamma}$ orginate from the one-loop contribution of the $H^\pm$ and large $|s_\delta|$. In the region resulting in large $\delta\mu_{Z\gamma}$, the recent constraint on the $\mu_{\gamma\gamma}$ always gives more strict upper bound on $\mu_{Z\gamma}$ than that obtained from recent experiments. In particular, our numerical investigation predicts $|\delta\mu_{Z\gamma}| \leq |\delta\mu_{\gamma\gamma}| < 0.23$, which is the sensitivity of $\mu_{Z\gamma}$ given in HL-LHC. On the other hand, in a model with $\beta = \sqrt{3}$ and $v_3 \simeq 3$ TeV, the allowed region $|\delta\mu_{\gamma\gamma}| = 0.04$ this model still allows $|\delta\mu_{Z\gamma}|$ to be close to 0.1, but it cannot reach the near future sensitivity $|\delta\mu_{Z\gamma}| = 0.23$. Theoretically, we have found two very interesting properties. First, $F_{21,sv}^{331}$ may have order of $F_{21,v}^{331}$ in allowed regions of the parameter space, so $F_{21,sv}^{331}$ should not be ignored as previous assmuptions. Second, one-loop contributions from gauge bosons can reach the order of charged Higgs contributions, leading to the existence of regions having respective destructive and constructive contributions to the decay amplitudes $h \to \gamma\gamma$ and $h \to Z\gamma$. This suggests that there may exist recent gauge extensions of the SM that allow large $|\delta\mu_{Z\gamma}|$ while still satisfy the future experimental data including $|\delta\mu_{\gamma\gamma}| \leq 0.04$.

**Conclusions:** Review the main obtained results and propose future research directions.

**Appendix:** We present some detailed intermediate steps related to the calculations in the main part of this thesis.

# Chapter 1

# THE 3-3-1 MODEL REVIEW

## 1.1 Limitations of the Standard model (SM)

The standard model (SM) has been very successful in unifying the interactions, fully describing the characteristics of masses and particle interactions, thereby making accurate predictions that have been verified and validated by experiment. However, SM still has limitations that we need to be overcome. Firstly, SM describes three types of interactions: strong, electromagnetic and weak interactions, but it does not include attractive interactions. Second, the SM describes neutrino as massless, in contrast to the discovery of atmospheric neutrino conversion in the Super Kamiokande (1998) experiment. This proves that there is a violation of the number of generational leptons in the neutral lepton region, in which this quantity is completely conserved. Third, although the Higgs boson has been observed by the LHC with a mass of about 125 GeV, many of its interaction features have not been concretely determined experimentally to be comparable to predictions by SM. Fourth, in SM, there is no theoretical basis or condition that forces the generation number of fermions to be 3, ... Therefore, building new models beyond the SM (BSM) is really necessary in order to solve problems that cannot be explained by SM. These BSM may also contains many new physical signals which can be tested by expereiments.

## 1.2 The 3-3-1 Flipped Models

The partical content is presented in Table 1.1. These Higgs bosons develop vacuum expectation values (VEV) defined as:

$$\begin{aligned}
\sigma_i^0 &= n_i + \frac{1}{\sqrt{2}}\left(R_{\sigma_i} + iI_{\sigma_i}\right), \quad \langle\sigma_i^0\rangle = n_i,\ i = 1, 2, S, \\
H_\alpha^0 &= k_\alpha + \frac{1}{\sqrt{2}}\left(R_\alpha + iI_\alpha\right), \quad \langle H_\alpha^0\rangle = k_\alpha,\ \alpha = 1, 2, 3, S, \\
\Delta^0 &= \epsilon_S + \frac{1}{\sqrt{2}}\left(R_\Delta + iI_\Delta\right), \quad \langle\Delta^0\rangle = \epsilon_S,
\end{aligned} \tag{1.1}$$

| Name | 3-3-1 rep | SM group decomposition | Components | # Flavors |
|---|---|---|---|---|
| $L_e$ | $(\mathbf{1},\mathbf{6},-\frac{1}{3})$ | $\left(\mathbf{1},\widehat{\mathbf{3}},0\right)+\left(\mathbf{1},\widehat{\mathbf{2}},-\frac{1}{2}\right)+\left(\mathbf{1},\widehat{\mathbf{1}},-1\right)$ | $\begin{pmatrix} (\Sigma^-)^c & \frac{1}{\sqrt{2}}\Sigma^0 & \frac{1}{\sqrt{2}}\nu_e \\ \frac{1}{\sqrt{2}}\Sigma^0 & \Sigma^- & \frac{1}{\sqrt{2}}e \\ \frac{1}{\sqrt{2}}\nu_e & \frac{1}{\sqrt{2}}e & E_e \end{pmatrix}_L$ | 1 |
| $L_{\alpha=\mu,\tau}$ | $(\mathbf{1},\mathbf{3},-\frac{2}{3})$ | $\left(\mathbf{1},\widehat{\mathbf{2}},-\frac{1}{2}\right)+\left(\mathbf{1},\widehat{\mathbf{1}},-1\right)$ | $(\nu_\alpha, e_\alpha, E_\alpha)^T_L$ | 2 |
| $e_{\alpha R}$ | $(\mathbf{1},\mathbf{1},-1)$ | $\left(\mathbf{1},\widehat{\mathbf{1}},-1\right)$ | $e_{\alpha R}$ | 6 |
| $Q_\alpha$ | $(\mathbf{3},\overline{\mathbf{3}},\frac{1}{3})$ | $\left(\mathbf{3},\widehat{\mathbf{2}},\frac{1}{6}\right)+\left(\mathbf{3},\widehat{\mathbf{1}},\frac{2}{3}\right)$ | $(d_\alpha, -u_\alpha, U_\alpha)^T_L$ | 3 |
| $u_{\alpha R}$ | $(\mathbf{3},\mathbf{1},\frac{2}{3})$ | $\left(\mathbf{3},\widehat{\mathbf{1}},\frac{2}{3}\right)$ | $u_{\alpha R}$ | 6 |
| $d_{\alpha R}$ | $(\mathbf{3},\mathbf{1},-\frac{1}{3})$ | $\left(\mathbf{3},\widehat{\mathbf{1}},-\frac{1}{3}\right)$ | $d_{\alpha R}$ | 3 |
| $\phi_{i=1,2}$ | $(\mathbf{1},\mathbf{3},\frac{1}{3})$ | $\left(\mathbf{1},\widehat{\mathbf{2}},\frac{1}{2}\right)+\left(\mathbf{1},\widehat{\mathbf{1}},0\right)$ | $\left(H_i^+, H_i^0, \sigma_i^0\right)^T$ | 2 |
| $\phi_3$ | $(\mathbf{1},\mathbf{3},-\frac{2}{3})$ | $\left(\mathbf{1},\widehat{\mathbf{2}},-\frac{1}{2}\right)+\left(\mathbf{1},\widehat{\mathbf{1}},-1\right)$ | $\left(H_3^0, H_3^-, \sigma_3^-\right)^T$ | 1 |
| $S$ | $(\mathbf{1},\mathbf{6},\frac{2}{3})$ | $\left(\mathbf{1},\widehat{\mathbf{3}},1\right)+\left(\mathbf{1},\widehat{\mathbf{2}},\frac{1}{2}\right)+\left(\mathbf{1},\widehat{\mathbf{1}},0\right)$ | $\begin{pmatrix} \Delta^{++} & \frac{1}{\sqrt{2}}\Delta^+ & \frac{1}{\sqrt{2}}H_S^+ \\ \frac{1}{\sqrt{2}}\Delta^+ & \Delta^0 & \frac{1}{\sqrt{2}}H_S^0 \\ \frac{1}{\sqrt{2}}H_S^+ & \frac{1}{\sqrt{2}}H_S^0 & \sigma_S^0 \end{pmatrix}$ | 1 |

Table 1.1: Representations for the flipped 3-3-1 model, notations of fermions are Dirac spinors.

The covariant derivative of the $SU(3)_L \times U(1)_X$ group is defined as below:

$$D_\mu \equiv \partial_\mu - igW_\mu^a T^a - ig_X T^9 X X_\mu, \tag{1.2}$$

where $T^a$ $(a = 1, 2, .., 8)$ are the $SU(3)$ generators with respective gauge boson $W_\mu^a$, $T^9 = \frac{I}{\sqrt{6}}$ is the $U(1)_X$ generator with the gauge boson $X_\mu$ and $X$ is the $U(1)_X$ charge of the field acted by the covariant derivative. Specific cases:

- For a $SU(3)_L$ singlet: $T^a = 0\ \forall a = 1, 2, .., 8$; the $U(1)_X$ generator: $T^9 = \frac{1}{\sqrt{6}}$.
- For a $SU(3)_L$ triplet: $T^a = \frac{1}{2}\lambda_a\ \forall a = 1, 2, .., 8$, $T^9 = \frac{1}{\sqrt{6}} I_3$, where $\lambda_a$ are Gell-Mann matrices. The covariant part can be written as:

$$\mathcal{W}_\mu \equiv W^a T^a = \frac{1}{2}\begin{pmatrix} W_\mu^3 + \frac{1}{\sqrt{3}}W_\mu^8 & \sqrt{2}W_\mu'^+ & \sqrt{2}Y_\mu'^+ \\ \sqrt{2}W_\mu^- & -W_\mu^3 + \frac{1}{\sqrt{3}}W_\mu^8 & \sqrt{2}V_\mu'^0 \\ \sqrt{2}Y_\mu^- & \sqrt{2}V_\mu'^{0*} & -\frac{2}{\sqrt{3}}W_\mu^8 \end{pmatrix},$$

$$W_\mu'^\pm = \frac{1}{\sqrt{2}}\left(W_\mu^1 \mp iW_\mu^2\right), \quad Y_\mu'^\pm = \frac{1}{\sqrt{2}}\left(W_\mu^4 \mp iW_\mu^5\right), \quad V_\mu'^0 = \frac{1}{\sqrt{2}}\left(W_\mu^6 - iW_\mu^7\right).$$

- For a $SU(3)_L$ antitriplets: $T^a = -\frac{1}{2}\lambda_a^* = -\frac{1}{2}\lambda_a^T\ \forall a = 1, 2, .., 8.$ $T^9 = \frac{1}{\sqrt{6}} I_3$.
- For a $SU(3)_L$ sextet denoted as $S \sim (6, 2/3)$, given in table 1.1, action of a $SU(3)_L$ generator can be written in terms of the Gellmann matrix, $T^a S = S\lambda_a/2 + \lambda_a/2 S^T$. The corresponding covariant derivative can be written in terms of the generators of the $SU(3)$ triplet

$$D_\mu S = \partial_\mu S - ig\left[SW_\mu + SW_\mu^T\right] - ig_X \frac{X}{\sqrt{6}} X_\mu S. \tag{1.3}$$

## 1.3 The 3-3-1 with arbitrary $\beta$

Left and right leptons are assigned to $SU(3)_L$ representations as follows:

$$L'_{aL} = \begin{pmatrix} e'_a \\ -\nu'_a \\ E'_a \end{pmatrix}_L \sim \left(1\ ,3^*\ ,-\frac{1}{2}+\frac{\beta}{2\sqrt{3}}\right), \quad a=1,2,3,$$
$$e'_{aR} \sim (1\ ,1\ ,-1)\,,\ \nu'_{aR} \sim (1\ ,1\ ,0)\,,\ E'_{aR} \sim \left(1\ ,1\ ,-\frac{1}{2}+\frac{\sqrt{3}\beta}{2}\right), \quad (1.4)$$

where numbers in the parentheses present the representations and the hypercharge $X$ of the gauge groups $SU(3)_C$, $SU(3)_L$ and $U(1)_X$, respectively.

The quark sector is arranged to guarantee anomaly cancellation, namely

$$Q'_{iL} = \begin{pmatrix} u'_i \\ d'_i \\ J'_i \end{pmatrix}_L \sim \left(3,\ 3\ ,\frac{1}{6}-\frac{\beta}{2\sqrt{3}}\right),\ Q'_{3L} = \begin{pmatrix} d'_3 \\ -u'_3 \\ J'_3 \end{pmatrix}_L \sim \left(3,\ 3^*\ ,\frac{1}{6}+\frac{\beta}{2\sqrt{3}}\right),$$
$$u'_{aR} \sim \left(3,\ 1\ ,\frac{2}{3}\right),\ d'_{aR} \sim \left(3,\ 1\ ,\frac{-1}{3}\right),\ J'_{iR} \sim \left(3,\ 1\ ,\frac{1}{6}-\frac{\sqrt{3}\beta}{2}\right),\ J'_{3R} \sim \left(3,\ 1\ ,\frac{1}{6}+\frac{\sqrt{3}\beta}{2}\right),$$

where $i=1,2$, $a=1,2,3$ v $J_{aL,R}$ are exotic quarks.

Three scalar triplets are introduced to generate masses for gauge bosons and fermions:

$$\chi = \begin{pmatrix} \chi^{+A} \\ \chi^{+B} \\ \chi^0 \end{pmatrix} \sim \left(1,\ 3\ ,\frac{\beta}{\sqrt{3}}\right),\ \rho = \begin{pmatrix} \rho^+ \\ \rho^0 \\ \rho^{-B} \end{pmatrix} \sim \left(1,\ 3\ ,\frac{1}{2}-\frac{\beta}{2\sqrt{3}}\right),$$
$$\eta = \begin{pmatrix} \eta^0 \\ \eta^- \\ \eta^{-A} \end{pmatrix} \sim \left(1,\ 3\ ,-\frac{1}{2}-\frac{\beta}{2\sqrt{3}}\right), \quad (1.5)$$

where, $A, B$ denote electric charges defined: $A=\frac{1+\beta\sqrt{3}}{2}$ and $B=\frac{-1+\beta\sqrt{3}}{2}$. These Higgs bosons develop vevs defined as $\langle\chi^0\rangle=\frac{v_3}{\sqrt{2}}$, $\langle\rho^0\rangle=\frac{v_2}{\sqrt{2}}$, $\langle\eta^0\rangle=\frac{v_1}{\sqrt{2}}$, leading to: $\chi^0=\frac{v_3+r_3+ia_3}{\sqrt{2}}$, $\langle\rho^0\rangle=\frac{v_2+r_2+ia_2}{\sqrt{2}}$, and $\eta^0\rangle=\frac{v_1+r_1+ia_1}{\sqrt{2}}$. The symmetry breaking happens in two steps: $SU(3)_L\otimes U(1)_X \xrightarrow{v_3} SU(2)_L\otimes U(1)_Y \xrightarrow{v_1,v_2} U(1)_Q$. It is therefore reasonable to assume that $v_3 > v_1, v_2$. At the second breaking step, $\rho$ and $\eta$ play roles of the two $SU(2)_L$ doublets, similarly to the case appearing in 2HDM.

# Chapter 2

# ANALYTIC FORMULAS FOR LFVHD IN THE FLIPPED 3-3-1 MODEL

## 2.1 LFV sources and the couplings related to the decay LFVHD

The following terms are involved with LFVHD couplings:

$$\begin{aligned}\mathcal{L}_{ffV}^{\text{LFV}} &= g\left[\overline{E_{eL}}\gamma^{\mu}e_L + \frac{1}{\sqrt{2}}\left(\overline{E_{\mu L}}\gamma^{\mu}\mu_L + \overline{E_{\tau L}}\gamma^{\mu}\tau_L\right)\right]V_{\mu}^{0} + \text{h.c.} \\ &= g\left[(V_L^{E*})_{3i}\overline{E_i}\gamma^{\mu}P_L e + \frac{1}{\sqrt{2}}\left[(V_L^{E*})_{1i}\overline{E_i}\gamma^{\mu}P_L\mu + (V_L^{E*})_{2i}\overline{E_i}\gamma^{\mu}P_L\tau\right]\right]V_{\mu}^{0} + \text{H.c.}.\end{aligned}$$

In the physical basis, the Yukawa couplings $\overline{f}fs^0$ involve LFVHD as below:

$$\begin{aligned}\mathcal{L}_{sff} = &-\frac{H_1^{0*}}{k_1}\left[m_{\mu}\overline{\mu_R}\mu_L + m_{\tau}\overline{\tau_R}\tau_L\right] - \sigma_1^0\sum_{i=1}^{3}\sum_{j=1,2}Y_{ji}^{\sigma_1^0}\overline{E_i}P_R e_{(j+1)} \\ &- h_6^*\sum_{i}^{3}\left[\sum_{j=1}^{2}Y_{ji}^{h_6}\overline{E_i}P_L e_{(j+1)} + Y_{3i}^{h_6}\overline{E_i}P_L e\right] + \text{H.c},\end{aligned} \tag{2.1}$$

where the coupling $Y_{ji}^{s}$, $i,j = 1,2,3$, is defined as follows:

$$Y_{ji}^{\sigma_1^0} = \begin{cases} \frac{m_{e_{(j+1)}}}{k_1}(V_L^{E*})_{ji}, & j = 1,2, \\ 0, & j = 3 \end{cases}, \quad Y_{ji}^{h_6} = s_{2s}Y_{ji}^{\ell};\ j = 1,2,3,\ s_{2s} = \frac{c_{2s}n_S}{n_2}. \tag{2.2}$$

The one-loop Feynman diagrams that contribute to the LFVHD amplitude are shown in Fig. 2.1.

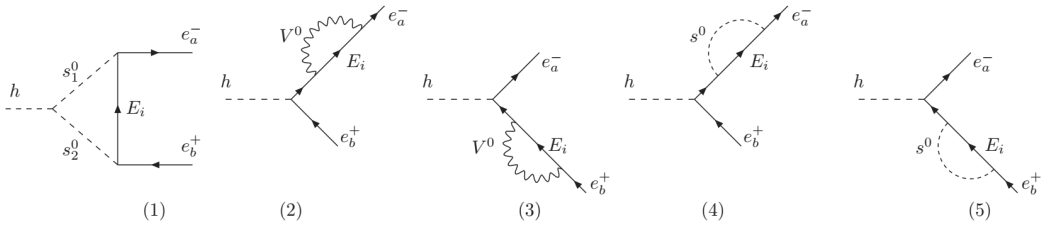


Figure 2.1: One-loop Feynman diagrams for decay $h \to e_a e_b$ in the unitary gauge, where $s^0, s_1^0, s_2^0 = h_6, \sigma_1^0$.

## 2.2 Analytical formulas of decay amplitude $h \to \mu\tau$

The partial decay width of the decays $h \to e_a e_b$ is defined as follows:

$$\Gamma(h \to e_a e_b) \equiv \Gamma(h \to e_a^- e_b^+) + \Gamma(h \to e_a^+ e_b^-) = \frac{m_h}{8\pi}\left(|\Delta_{(ba)L}|^2 + |\Delta_{(ba)R}|^2\right),$$

with the condition $m_h \gg m_{a,b}$ and $m_{a,b}$ charged lepton, $a, b = 1, 2, 3$ corresponding to $e, \mu, \tau$. The LFVHD decay rate is $\mathrm{BR}(h \to e_a e_b) = \Gamma(h \to e_a e_b)/\Gamma_h^{\mathrm{total}}$ where $\Gamma_h^{\mathrm{total}} = 4.1 \times 10^{-3}$ GeV. The $\Delta_{(ba)L,R}$ can be written as:

$$\Delta_{(ba)L,R} = \sum_{i=1}^{5} \Delta^{(i)}_{(ba)L,R}. \tag{2.3}$$

We focus only to $\Delta^{(1)}_{(ba)L,R} = \Delta_{(ba)L,R}$ with the following main contribution:

$$\Delta_{(32)L,R} = \Delta^{\sigma_1^0\sigma_1^0}_{(32)L,R} + \Delta^{\sigma_1^0 h_6}_{(32)L,R} + \Delta^{h_6\sigma_1^0}_{(32)L,R},\ \Delta_{(b1)L,R} = \Delta^{\sigma_1^0 h_6}_{(b1)L,R},\ b = 2, 3,$$

$$\Delta^{\sigma_1^0\sigma_1^0}_{(32)L} = \frac{m_\tau \lambda_{13} m_W}{16\pi^2 g} \times \sum_{i=1}^{3} Y_{1i}^{\sigma_1^0 *} Y_{2i}^{\sigma_1^0} \left[-C_2(0,0; m_{E_i}^2, m_{\sigma_1^0}^2, m_{\sigma_1^0}^2)\right],$$

$$\Delta^{\sigma_1^0\sigma_1^0}_{(32)R} = \frac{m_\mu \lambda_{13} m_W}{16\pi^2 g} \times \sum_{i=1}^{3} Y_{1i}^{\sigma_1^0 *} Y_{2i}^{\sigma_1^0} \left[C_1(0,0; m_{E_i}^2, m_{\sigma_1^0}^2, m_{\sigma_1^0}^2)\right],$$

$$\Delta^{\sigma_1^0 h_6}_{(32)L} = -\frac{f^\phi s_{2s}}{32\pi^2} \times \sum_{i=1}^{3} Y_{1i}^{\sigma_1^0 *} Y_{2i}^{h_6} \left[m_{E_i} C_0(0,0; m_{E_i}^2, m_{\sigma_1^0}^2, m_{h_6}^2)\right],$$

$$\Delta^{h_6\sigma_1^0}_{(32)R} = -\frac{f^\phi s_{2s}}{32\pi^2} \times \sum_{i=1}^{3} Y_{1i}^{\sigma_1^0} Y_{2i}^{h_6 *} \left[m_{E_i} C_0(0,0; m_{E_i}^2, m_{h_6}^2, m_{\sigma_1^0}^2)\right],$$

$$\Delta^{\sigma_1^0 h_6}_{(b1)R} = -\frac{f^\phi s_{2s}}{32\pi^2} \times \sum_{i=1}^{3} Y_{3i}^{\sigma_1^0} Y_{(b-1)i}^{h_6 *} \left[m_{E_i} C_0(0,0; m_{E_i}^2, m_{h_6}^2, m_{\sigma_1^0}^2)\right],$$

where $C_{0,1,2}$ are one-loop three-point Passarino-Veltman (PV) functions.

In the unitary gauge, the one-loop three point Feynman diagrams contributing to the decay amplitudes $e_b \to e_a \gamma$ $(a < b)$ are shown in Fig. 2.2. For low energy, the

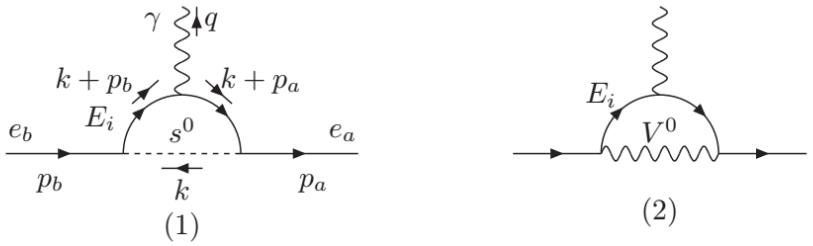


Figure 2.2: One-loop diagrams contributing to $C_{(ba)L,R}$ for decays $e_b \to e_a\gamma$, where $s^0 = \sigma_1^0, h_6$.

branching ratios of the cLFV decays can be written in a more convinient form as follows:

$$\mathrm{BR}(e_b \to e_a\gamma) = \left(1 - \frac{m_a^2}{m_b^2}\right)^3 \times \frac{3\alpha_e}{2\pi}\left(\left|F_{(ba)L}\right|^2 + |F_{(ba)R}|^2\right) \times \mathrm{BR}(e_b \to e_a\bar{\nu}_a\nu_b),$$

where $\alpha_e \simeq 1/137$, $F_{(ba)L,R} = \frac{C_{(ba)L,R}}{m_b} \times \left(\frac{g^2 e}{32\pi^2 m_W^2}\right)^{-1}$ and $C_{(ba)L,R}$ is the one loop contributions originated from diagrams shown in Fig. 2.2. The well-known experimental values of $\mathrm{BR}(e_b \to e_a\bar{\nu}_a\nu_b)$ are $\mathrm{BR}(\tau \to \mu\bar{\nu}_\mu\nu_\tau) \simeq 17.41\%$, $\mathrm{BR}(\tau \to e\bar{\nu}_e\nu_\tau) \simeq 17.83\%$ v $\mathrm{BR}(\mu \to e\bar{\nu}_e\nu_\mu) \simeq 100\%$. Using the limit $m_a^2, m_b^2 \simeq 0$, the results are as follows:

$$\begin{aligned}
F_{(ba)L,R} &= F^{(1)}_{(ba)L,R} + F^{(2)}_{(ba)L,R},\\
F^{(1)}_{(32)L} &= \sum_{i=1}^{3} \frac{2m_W^2 Y^{\sigma_1^0 *}_{1i} Y^{\sigma_1^0}_{2i}}{g^2 m^2_{\sigma_1^0}} g_s(t_{\sigma_1^0,i}) + \sum_{i=1}^{3} \frac{2m_\mu m_W^2 Y^{h_6 *}_{1i} Y^{h_6}_{2i}}{m_\tau g^2 m^2_{h_6}} g_s(t_{h_6,i}),\\
F^{(1)}_{(32)R} &= \sum_{i=1}^{3} \frac{2m_\mu m_W^2 Y^{\sigma_1^0 *}_{1i} Y^{\sigma_1^0}_{2i}}{m_\tau g^2 m^2_{\sigma_1^0}} g_s(t_{\sigma_1^0,i}) + \sum_{i=1}^{3} \frac{2m_W^2 Y^{h_6 *}_{1i} Y^{h_6}_{2i}}{g^2 m^2_{h_6}} g_s(t_{h_6,i}),\\
F^{(1)}_{(b1)L} &= \frac{m_e}{m_b} F^{(1)}_{(b1)R} = \sum_{i=1}^{3} \frac{2m_e m_W^2 Y^{h_6 *}_{3i} Y^{h_6}_{(b-1)i}}{m_b g^2 m^2_{h_6}} g_s(t_{h_6,i}),\\
F^{(2)}_{(32)L} &= \frac{m_\mu}{m_\tau} F^{(2)}_{(32)R} = \frac{2m_W^2}{m^2_{V^0}} \sum_{i=1}^{3} V'^E_{1i} V'^{E*}_{2i} g_v(t_{v,i}),\\
F^{(2)}_{(b1)L} &= \frac{m_e}{m_b} F^{(2)}_{(b1)R} = \frac{2m_W^2}{m^2_{V^0}} \sum_{i=1}^{3} V'^E_{3i} V'^{E*}_{(b-1)i} g_v(t_{v,i}),
\end{aligned} \tag{2.4}$$

where $t_{x,i} = m^2_{E_i}/m^2_x$ $(x = \sigma_1^0, h_6, V^0)$,

$$V'^E_{ai} = \begin{cases} (V_L^E)_{ai}, & a = 3 \\ \frac{1}{\sqrt{2}}(V_L^E)_{ai}, & a = 1, 2 \end{cases}, \tag{2.5}$$

and $g_s(t_{s,i})$, $g_v(t_{v,i})$ are known functions . We note that $\sigma_1^0$ contribute to only LFV decay $\tau \to \mu\gamma$ and $h \to \mu\tau$.

# Chapter 3

# NUMERICAL RESULTS AND DISCUSSIONS FOR DECAY $h \to \mu\tau$ IN THE FLIPPED 3-3-1 MODEL

## 3.1 Constraints of the parameters space

In this numerical discussion, the unknown input parameters are: $m_{E_i}$ and $s^E_{ij}$; $m_{\sigma^0_1}$, $m_{h_6}$ and $s_{2s}$; $k_1$ and $n_2$. The related dependent parameters are

$$n_S = \frac{s_{2s} n_2}{c_{2s}\sqrt{2}}, \quad n_2^2(1 + 2t_{2s}^2) = \frac{(3 - 4s_W^2)m_{Z'}^2}{4g^2 c_W^2}, \tag{3.1}$$

where $t_{2s} \equiv s_{2s}/c_{2s}$. This means that $n_2^2 + 4n_S^2 \simeq (2.15 m_{Z'})^2$. For the latest lower bound of $m_{Z'}^2 \geq 4$ TeV for $\sqrt{n_2^2 + 4n_S^2} \geq 8.3$ TeV. For our numerical investigation, we will fix $\sqrt{n_2^2 + 4n_S^2} = 8.3$ TeV, $n_2 = 1$ TeV, $n_S \geq 4$ TeV, leading to $t_{2s} = \sqrt{2} n_S/n_2 = 4\sqrt{2}$, equivalently $s_{2s} \simeq 0.985$. The large $s_{2s}$ corresponds to large Yukawa coupling $Y^{h_6}$ given in Eq. (2.2). Hence we will choose that 10 GeV $\leq k_1 \leq$ 50 GeV. Choosing of $m_{E_i}$ allow large BR($h \to e_b e_a$): $m_{E_i} - m_{E_j} = \mathcal{O}(10^2)$ GeV.

The default values of the inputs are $k_1 = 20$ GeV, $\lambda_{13} = 1$, $f^\phi = 2$ TeV, $m_{E_1} = 1$ TeV, $m_{E_k} = m_{E_1} - k \times 100$ GeV, $n_2 = 1$ TeV, $s_{2s} = 0.985$, $m_{\sigma^0_1} = m_{h_6} = 1$ TeV. The perturbative limit of the Yukawa couplings relating with heavy lepton masses gives $m_{E_1} \leq n_2\sqrt{4\pi} = 3.5$ TeV for $n_2 = 1$ TeV. All other well-known parameters are: $m_h = 125.01$ GeV and total decay width $\Gamma_h = 4.07 \times 10^{-3}$ GeV; $m_W$, $m_e$, $m_\mu$, $m_\tau$, the gauge couplings and $\alpha_e$.

## 3.2 Numerical results and discussion

In the case of $s_{12} = 1/\sqrt{2}$ and $s_{13} = s_{23} = 0$, we always have BR($h \to \mu e$) = BR($h \to \tau e$) = BR($\mu \to e\gamma$) = BR($\tau \to e\gamma$) = 0. In contrast, the BR($h \to \tau\mu$) and BR($\tau \to \mu\gamma$) may be large and drawn as a function of $m_{E_1}$ with different fixed $k_1$. The numerical results are shown in Fig 3.1. It can be seen that BR($\tau \to \mu\gamma$) is much smaller than the current experimental

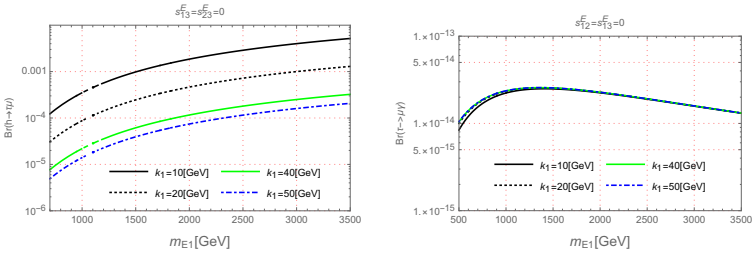


Figure 3.1: BR($h \to \tau\mu$) and BR($\tau \to \mu\gamma$) as functions of $m_{E_1}$ in the case $s^E_{12} = \frac{1}{\sqrt{2}}$, $s^E_{13} = s^E_{23} = 0$.

bound. The BR($h \to \tau\mu$) $\sim \mathcal{O}(10^{-3})$ is close to the current experimental bound. the lower bounds obtained from near future experiments can be used to constrain the parameter space of the model. The two parameters $k_1$ and $m_{E_1}$ affect strongly on BR($h \to \tau\mu$).

Similarly, with $s^E_{12} = s^E_{23} = 0$ and $s^E_{13} = \frac{1}{\sqrt{2}}$, illustrations of these branching ratios as functions of $m_{E_1}$ with different fixed $k_1$ are shown in Fig. 3.2. Accordingly, BR($\mu \to e\gamma$) $\leq$

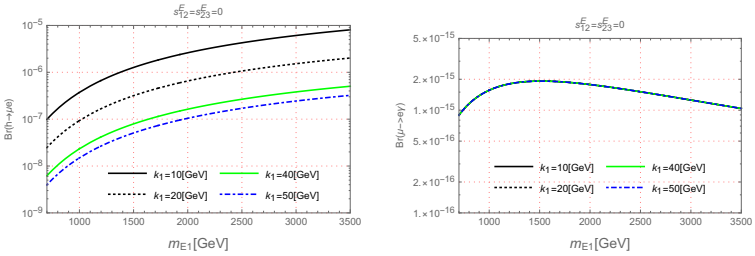


Figure 3.2: BR($h \to \mu e$) and BR($\mu \to e\gamma$) as functions of $m_{E_1}$ in the case $s^E_{13} = \frac{1}{\sqrt{2}}$ and $s^E_{12} = s^E_{13} = 0$.

$\mathcal{O}(10^{-15})$, which still satisfies the uppep experimental bound. It is noted that although BR($h \to \mu e$) is sensitive to $k_1$, the BR($\mu \to e\gamma$) is not, because it does not receive contribution from Yukawa coupling of $\sigma^0_1$.

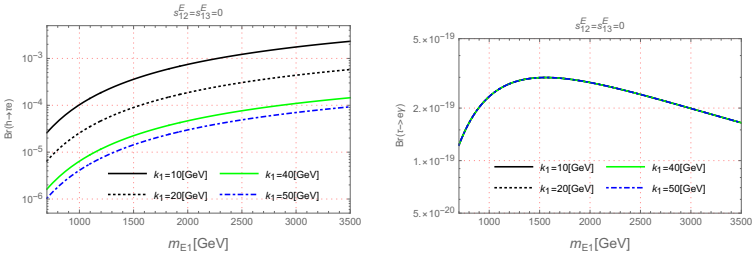


Figure 3.3: BR($h \to \tau e$) and BR($\tau \to e\gamma$) as functions of $m_{E_1}$ in the case $s^E_{23} = \frac{1}{\sqrt{2}}$ and $s^E_{12} = s^E_{13} = 0$.

The case of $s^E_{12} = s^E_{13} = 0$ and $s^E_{23} = \frac{1}{\sqrt{2}}$, illustrations of these branching ratios as functions of $m_{E_1}$ with different fixed $k_1$ are shown in Fig. 3.3. The BR($h \to \tau e$) has the same order of BR($h \to \tau\mu$), because both of them get dominant contributions from $\Delta^{\sigma^0_1 h_6}_{(ba)R}$. The BR($\tau \to e\gamma$) is much smaller than the current and upcoming experimental sensitivities.

# Chapter 4

# ANALYSIS OF RESULTS FOR DECAYS $h \to Z\gamma, \gamma\gamma$ IN THE 3-3-1 MODEL WITH ARBITRARY $\beta$

## 4.1 The couplings related to the decays $h \to Z\gamma, \gamma\gamma$

Feynman rules for the SM-like Higgs boson coupling with charged Higgs bosons related to the decays $h \to Z\gamma$ and $h \to \gamma\gamma$ are shown in Table 4.1.

| Vertex | Coupling: $-i\lambda_{hss}$ |
|---|---|
| $-i\lambda_{hH^+H^-}$ | $iv\left[2s_{12}c_{12}\left(-\lambda_1 c_{12}\, c_\alpha + \lambda_2 s_{12}\, s_\alpha\right) + \left(s_\alpha c_{12}^3 - c_\alpha s_{12}^3\right)\lambda_{12} - c_\delta \tilde{\lambda}_{12}\right]$ |
| $-i\lambda_{hH^AH^{-A}}$ | $ic_{13}^2\left\{v\left[s_\alpha c_{12}\left(\lambda_{12} + t_{13}^2\lambda_{23}\right) - c_\alpha s_{12}\left(2\lambda_1 + t_{13}^2(\lambda_{13} + \tilde{\lambda}_{13})\right)\right] + v_3 t_{13}\left(\frac{2fs_\alpha}{v_3} - c_\alpha\tilde{\lambda}_{13}\right)\right\}$ |
| $-i\lambda_{hH^BH^{-B}}$ | $ic_{23}^2\left\{v\left[s_\alpha c_{12}\left(2\lambda_2 + t_{23}^2(\lambda_{23} + \tilde{\lambda}_{23})\right) - c_\alpha s_{12}\left(\lambda_{12} + t_{23}^2\lambda_{13}\right)\right] + v_3 t_{23}\left(s_\alpha\tilde{\lambda}_{23} - \frac{2fc_\alpha}{v_3}\right)\right\}$ |

Table 4.1: Feynman rules for the SM-like Higgs boson couplings with charged Higgs bosons

The Yukawa coupling of the SM-like Higgs boson with fermion in SM are shown in Table 4.2. The Feynman rules: $-i\left(Y_{h\bar{f}f_L}P_L + Y_{h\bar{f}f_R}P_R\right)$ for each coupling $h\bar{f}f$. Both

| $-iY_{h\overline{e_a}e_aL,R}$ | $-iY_{h\overline{u_i}u_iL,R}$ | $-iY_{h\overline{u_3}u_3L,R}$ | $-iY_{h\overline{d_i}d_iL,R}$ | $-iY_{h\overline{d_3}d_3L,R}$ |
|---|---|---|---|---|
| $-i\frac{m_{e_a}}{v}\left(c_\delta - \frac{s_\delta}{t_{12}}\right)$ | $-i\frac{m_{u_i}}{v}\left(c_\delta - \frac{s_\delta}{t_{12}}\right)$ | $-i\frac{m_{u_3}}{v}\left(c_\delta + t_{12}s_\delta\right)$ | $-i\frac{m_{d_i}}{v}\left(c_\delta + t_{12}s_\delta\right)$ | $-i\frac{m_{d_3}}{v}\left(c_\delta - \frac{s_\delta}{t_{12}}\right)$ |

Table 4.2: Yukawa couplings of the SM-like Higgs boson

neutral Higgs bosons $h$ and $h_2^0$ do not couple to exotic fermions. In contrast, $h_3^0$ couples only to the exotic fermions, while does not couple to the SM ones.

The couplings of Higgs and gauge bosons arise from Lagrangian:

$$\mathcal{L}_{\text{kin}}^H = \sum_v g_{hvv}g_{\mu\nu}hv^{-Q\mu}v^{Q\nu} + \sum_{s,v}\left[-ig_{hsv}^*v^{-Q\mu}\left(s^{+Q}\partial_\mu h - h\partial_\mu s^{+Q}\right)h.c.\right]$$
$$+ \sum_s ig_{Zss}Z^\mu\left(s^{-Q}\partial_\mu s^Q - s^Q\partial_\mu s^{-Q}\right) + \sum_s ieQA^\mu\left(s^{-Q}\partial_\mu s^Q - s^Q\partial_\mu s^{-Q}\right)$$

$$+\sum_{s,v}\left[ig_{Zvs}Z^{\mu}v^{Q\nu}s^{-Q}g_{\mu\nu}+ig^{*}_{Zvs}Z^{\mu}v^{-Q\nu}s^{Q}g_{\mu\nu}\right]+..., \tag{4.1}$$

where $s = H^{\pm}, H^{\pm A}, H^{\pm B}$ and $v = W, Y, V$. We only list the relevant terms contributing to the decays $h \to Z\gamma, \gamma\gamma$ and ignore the remaining terms. The Feynman rules for particular couplings are shown in Table 4.3, where $\partial_\mu h \to -ip_{0\mu}h$ and $\partial_\mu s^{\pm Q} \to -ip_{\pm\mu}s^{\pm Q}$. The notations $p_0$, $p_\pm$ are incoming monenta of $h$ and $s^{\pm}$.

| Vertex | Coupling: | Vertex | Coupling |
|---|---|---|---|
| $g_{hW^+W^-}$ | $g\, m_W\, c_\delta$ | $g_{hY^+{}^AY^-{}^A}$ | $g\, m_W\, c_\alpha s_{12}$ |
| $g_{hV^+{}^BV^-{}^B}$ | $-g\, m_W\, s_\alpha c_{12}$ | $g_{hH^-W^+}$ | $\frac{g\, s_\delta}{2}$ |
| $g_{hH^-{}^AY^A}$ | $-\frac{g\, c_{13}c_\alpha}{2}$ | $g_{hH^-{}^BV^B}$ | $\frac{g\, c_{23}s_\alpha}{2}$ |

Table 4.3: Feynman rules for couplings of the SM-like Higgs boson to Higgs and gauge bosons.

The Feynman rules for the couplings of $Z$ to charged Higgs and gauge bosons in (4.1) are given in Table 4.4.

| Vertex | Coupling |
|---|---|
| $g_{ZH^+H^-}$ | $\frac{g}{2c_W}\left(c_\theta\, c_{2W}+\frac{s_\theta\left[\sqrt{3}c_W^2(1-2s_{12}^2)+3\beta s_W^2\right]}{3c_W\sqrt{1-\beta^2t_W^2}}\right)$ |
| $g_{ZH^A H^{-A}}$ | $\frac{g}{2c_W}\left(c_\theta\left[s_{13}^2-(1+\sqrt{3}\beta)s_W^2\right]+\frac{s_\theta\left[\sqrt{3}c_W^2(s_{13}^2-2)+3\beta(\sqrt{3}\beta+c_{13}^2)s_W^2\right]}{3c_W\sqrt{1-\beta^2t_W^2}}\right)$ |
| $g_{ZH^B H^{-B}}$ | $\frac{ig}{2c_W}\left(-c_\theta\left[s_{23}^2+(\sqrt{3}\beta-1)s_W^2\right]+\frac{s_\theta\left[\sqrt{3}c_W^2(s_{23}^2-2)+3\beta(\sqrt{3}\beta-c_{23}^2)s_W^2\right]}{3c_W\sqrt{1-\beta^2t_W^2}}\right)$ |
| $g_{ZW^+H^-}$ | $-\frac{g\, m_W(2s_{12}c_{12}s_\theta)}{\sqrt{3(1-\beta^2t_W^2)}}$ |
| $g_{ZY^A H^{-A}}$, $g_{ZY^{-A}H^A}$ | $\frac{g^2c_{13}}{4}\Big\{c_\theta c_W\left[s_{12}\left(1+(2+\sqrt{3}\beta)t_W^2\right)v+t_{13}(1-\sqrt{3}\beta t_W^2)v_3\right]$ $+\frac{s_\theta}{3\sqrt{1-\beta^2t_W^2}}\left[s_{12}\left(\sqrt{3}-3\beta(2+\sqrt{3}\beta)t_W^2\right)v+\sqrt{3}t_{13}\left(1+3\beta^2t_W^2\right)v_3\right]\Big\}$ |
| $g_{ZV^B H^{-B}}$, $g_{ZV^{-B}H^B}$ | $\frac{g^2c_{23}}{4}\Big\{c_\theta c_W\left[c_{12}\left(-1+(-2+\sqrt{3}\beta)t_W^2\right)v-t_{23}(1+\sqrt{3}\beta t_W^2)v_3\right]$ $+\frac{s_\theta}{3\sqrt{1-\beta^2t_W^2}}\left[c_{12}\left(\sqrt{3}-3\beta(-2+\sqrt{3}\beta)t_W^2\right)v+\sqrt{3}t_{23}\left(1+3\beta^2t_W^2\right)v_3\right]\Big\}$ |

Table 4.4: Feynman rules of couplings with $Z$ to charged Higgs and gauge bosons.

The couplings of $Z$ and photon $A_\mu$ with fermions arise from Lagrangian:

$$\mathcal{L}^f_{\rm kin}\supset\sum_f\left[\frac{g\, c_\theta}{c_W}\overline{f}\gamma^\mu\left(g_L^fP_L+g_R^fP_R\right)fZ_\mu+eQ_f\overline{f}\gamma^\mu fA_\mu\right], \tag{4.2}$$

where $f$ runs over all fermions in the 3-3-1$\beta$ model, $Q_f$ is the electric charge of the fermion $f$. Values of $g^f_{L,R}$ are shown in Table 4.5.

The triple couplings of three gauge bosons arise from:

$$\mathcal{L}^g_D=-\frac{1}{4}\sum_{a=1}^{8}F^a_{\mu\nu}F^{a\mu\nu}, \tag{4.3}$$

| $f$ | $g_L^f$ | $g_R^f$ |
|---|---|---|
| $e_a$ | $-\frac{1}{2}+s_W^2+\frac{t_\theta\, c_W(1-\sqrt{3}\beta t_W^2)}{2\sqrt{3(1-\beta^2t_W^2)}}$ | $s_W^2\left(1-\frac{t_\theta\,\beta}{c_W\sqrt{1-\beta^2t_W^2}}\right)$ |
| $u_i$ | $\frac{1}{2}-\frac{2}{3}s_W^2+\frac{t_\theta\, c_W(\beta t_W^2-\sqrt{3})}{6\sqrt{1-\beta^2t_W^2}}$ | $-\frac{2}{3}s_W^2\left(1-\frac{t_\theta\,\beta}{c_W\sqrt{1-\beta^2t_W^2}}\right)$ |
| $u_3$ | $\frac{1}{2}-\frac{2}{3}s_W^2+\frac{t_\theta\, c_W(\beta t_W^2+\sqrt{3})}{6\sqrt{1-\beta^2t_W^2}}$ | $-\frac{2}{3}s_W^2\left(1-\frac{t_\theta\,\beta}{c_W\sqrt{1-\beta^2t_W^2}}\right)$ |
| $d_i$ | $-\frac{1}{2}+\frac{1}{3}s_W^2+\frac{t_\theta c_W(\beta t_W^2-\sqrt{3})}{6\sqrt{1-\beta^2t_W^2}}$ | $\frac{1}{3}s_W^2\left(1-\frac{t_\theta\,\beta}{c_W\sqrt{1-\beta^2t_W^2}}\right)$ |
| $d_3$ | $-\frac{1}{2}+\frac{1}{3}s_W^2+\frac{t_\theta c_W(\beta t_W^2+\sqrt{3})}{6\sqrt{1-\beta^2t_W^2}}$ | $\frac{1}{3}s_W^2\left(1-\frac{t_\theta\,\beta}{c_W\sqrt{1-\beta^2t_W^2}}\right)$ |

Table 4.5: Couplings of $Z$ with fermions

where

$$F^a_{\mu\nu}=\partial_\mu W^a_\nu-\partial_\nu W^a_\mu+g\sum_{b,c=1}^{8}f^{abc}W^b_\mu W^c_\nu, \tag{4.4}$$

$f^{abc}$ $(a,b,c=1,2,...,8)$ are $SU(3)$ structure constants. The couplings are defined as:

$$\begin{aligned}\mathcal{L}^g_D\rightarrow&-g_{Zvv}Z^\mu(p_0)v^{+Q\nu}(p_+)v^{-Q\lambda}(p_-)\times\Gamma_{\mu\nu\lambda}(p_0,p_+,p_-),\\&-eQA^\mu(p_0)v^{+Q\nu}(p_+)v^{-Q\lambda}(p_-)\times\Gamma_{\mu\nu\lambda}(p_0,p_+,p_-),\end{aligned} \tag{4.5}$$

where $\Gamma_{\mu\nu\lambda}(p_0,p_+,p_-)\equiv g_{\mu\nu}(p_0-p_+)_\lambda+g_{\nu\lambda}(p_+-p_-)_\mu+g_{\lambda\mu}(p_--p_0)_\lambda$ and $v=W,V,Y$. The involved couplings of $Z$ are given in Table 4.6.

| Vertex | Coupling |
|---|---|
| $-ig_{ZW^{+\nu}W^{-\lambda}}$ | $-igc_Wc_\theta$ |
| $-ig_{ZY^AY^{-A}}$ | $\frac{ig}{2}\left[c_\theta\left(-c_W+\sqrt{3}\beta s_Wt_W\right)+s_\theta\sqrt{3-3\beta^2t_W^2}\right]$ |
| $-ig_{ZV^BY^{-B}}$ | $\frac{ig}{2}\left[c_\theta\left(c_W+\sqrt{3}\beta s_Wt_W\right)+s_\theta\sqrt{3-3\beta^2t_W^2}\right]$ |

Table 4.6: Feynman rules for triple gauge couplings relating with the decay $h\rightarrow Z\gamma,\gamma\gamma$.

## 4.2 Analytic formulas of the amplitude of the decays $h\rightarrow Z\gamma,\gamma\gamma$

In the unitary gauge, the above couplings generate one-loop three point Feynman diagrams contributing to the decay amplitude $h\rightarrow Z\gamma$, as given in Fig. 4.1. The partial decay width is

$$\Gamma(h\rightarrow Z\gamma)=\frac{m_h^3}{32\pi}\times\left(1-\frac{m_Z^2}{m_h^2}\right)^3|F_{21}|^2, \tag{4.6}$$

where $F_{21}$ is sum of all one-loop contributions corresponding to all diagrams:

$$F_{21}^{331}=\sum_f F_{21,f}^{331}+\sum_s F_{21,s}^{331}+\sum_v F_{21,v}^{331}+\sum_{\{s,v\}}\left(F_{21,vss}^{331}+F_{21,svv}^{331}\right). \tag{4.7}$$

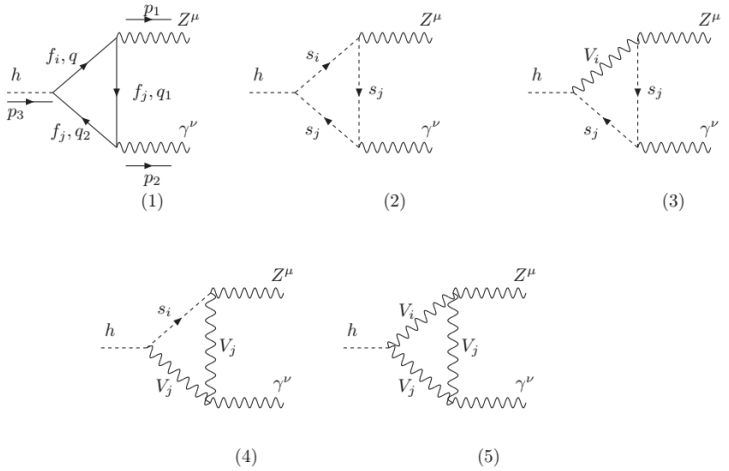


Figure 4.1: One-loop three-point Feynman diagrams contributing to the decay $h \to Z\gamma$ in the unitary gauge, where $f_{i,j}$ are the SM leptons, $s_{i,j} = H^\pm, H^{\pm A}, H^{\pm B}$, $v_{i,j} = W^\pm, Y^{\pm A}, V^{\pm B}$.

The partial decay width of the decay $h \to \gamma\gamma$ can be calculated as

$$\Gamma(h \to \gamma\gamma) = \frac{m_h^3}{64\pi} \times |F_{\gamma\gamma}^{331}|^2, \quad F_{\gamma\gamma}^{331} = \sum_f F_{\gamma\gamma,f}^{331} + \sum_s F_{\gamma\gamma,s}^{331} + \sum_v F_{\gamma\gamma,v}^{331}. \tag{4.8}$$

To determine the BR of a SM-like Higgs decay, we need to know the total decay width $\Gamma_h^{\rm SM}$. The BR of a particular decay channel $h \to XX$, $XX = gg, \gamma\gamma, Z\gamma$:

$$\mathrm{BR}^{\rm SM}(h \to XX) \equiv \frac{\Gamma^{\rm SM}(h \to XX)}{\Gamma_h^{\rm SM}}. \tag{4.9}$$

The respective signal strength of one loop-induced predicted by $3-3-1\beta$ is defined as:

$$\mu_X^{331} \equiv (c_\delta + t_{12}s_\delta)^2 \times \frac{\mathrm{BR}^{331}(h \to XX)}{\mathrm{BR}^{\rm SM}(h \to XX)}. \tag{4.10}$$

The recent signal strengths of the two loop-induced decays $h \to Z\gamma, \gamma\gamma$ are: $\mu_{Z\gamma} < 6.6(5.2)$ and $\mu_{\gamma\gamma} = 0.99 \pm 0.14$.

### Decays of the neutral Higgs boson $h_3^0$

The couplings of neutral heavy Higgs bosons $h_{2,3}^0$ to fermions are:

$$Y_{h_2^0 ffL,R} = \begin{cases} \frac{m_f}{v}\left(\frac{c_\delta}{t_{12}} + s_\delta\right), & f = e_a, u_i, d_3 \\ \frac{m_f}{v}\left(-c_\delta t_{12} + s_\delta\right), & f = u_3, d_i \\ 0, & f = E_a, J_a. \end{cases}, \; Y_{h_3^0 ffL,R} = \begin{cases} 0 & f = e_a, u_a, d_a \\ \frac{m_f}{v_3} & f = E_a, J_a \end{cases}.$$

The neutral Higgs boson $h_3^0$ that has only one non-zero Yukawa coupling with exotic fermions. The partial decay width $h_3^0 \to gg$ in the limit $t_a \gg 1 \; \forall a = 1, 2, 3$

$$\Gamma(h_3^0 \to gg) \simeq \frac{\alpha_s^2 m_{h_3^0}^3}{8\pi^3 v_3^2}. \tag{4.11}$$

The partial width of the tree level decay $h_3^0 \to hh$ when $m_{h_3^0} > 2m_h$ is:

$$\Gamma(h_3^0 \to hh) = \frac{|\lambda_{h_3^0 hh}|^2}{8\pi\, m_{h_3^0}} \sqrt{1 - \frac{4m_h^2}{m_{h_3^0}^2}} = \frac{\lambda_{13}^2 s_\delta^4 v_3^2}{8\pi\, c_{12}^4\, m_{h_3^0}} \sqrt{1 - \frac{4m_h^2}{m_{h_3^0}^2}}. \tag{4.12}$$

The total decay width of the $h_3^0$ is $\Gamma_{h_3^0} = \Gamma(h_3^0 \to\ hh) + \Gamma(h_3^0 \to\ gg) + \Gamma(h_3^0 \to\ \gamma\gamma) + \Gamma(h_3^0 \to\ Z\gamma)$. The other two partial decay widths are defined as follows:

$$\Gamma(h_3^0 \to Z\gamma) = \frac{m_{h_3^0}^3}{32\pi} \left(1 - \frac{m_Z^2}{m_{h_3^0}^2}\right)^3 |F_{21}(h_3^0 \to\ Z\gamma)|^2,\ \Gamma(h_3^0 \to \gamma\gamma) = \frac{m_{h_3^0}^3}{64\pi} |F_{\gamma\gamma}^{331}(h_3^0 \to \gamma\gamma)|^2,$$

$$\begin{aligned} F_{21}^{331}(h_3^0 \to\ Z\gamma) = &\sum_{F=E_a,J_a} F_{21,F}^{331}(h_3^0 \to\ Z\gamma) + \sum_s F_{21,s}^{331}(h_3^0 \to\ Z\gamma) + \sum_{v=Y,V} F_{21,v}^{331}(h_3^0 \to\ Z\gamma) \\ &+ \sum_{\{s,v\}} \left[F_{21,vss}^{331}(h_3^0 \to\ Z\gamma) + F_{21,svv}^{331}(h_3^0 \to\ Z\gamma)\right], \end{aligned} \tag{4.13}$$

$$F_{\gamma\gamma}^{331}(h_3^0 \to\ \gamma\gamma) = \sum_{F=E_a,J_a} F_{\gamma\gamma,F}^{331}(h_3^0 \to\ Z\gamma) + \sum_s F_{\gamma\gamma,s}^{331}(h_3^0 \to\ Z\gamma) + \sum_{v=Y,V} F_{\gamma\gamma,v}^{331}(h_3^0 \to\ Z\gamma),$$

where $s = H^\pm, H^{\pm,A}, H^{\pm,B}$, $v = Y^{\pm,A}, V^{\pm,B}$ v $\{s,v\} = \{H^{\pm,A}, Y^{\pm,A}\}, \{H^{\pm,B}, V^{\pm,B}\}$..

# Chapter 5

# NUMERICAL DISCUSSIONS OF THE DECAYS $h \to Z\gamma, \gamma\gamma$ IN THE 3-3-1 MODEL WITH ARBITRARY $\beta$

## 5.1 Constraints of the parameter space

To investigate quantitative deviations between predictions of the two models 3-3-1$\beta$ and the SM for decays $h \to X$ ($X = \gamma\gamma, Z\gamma$), we define a quantity $\delta\mu_X$ as follows $\delta\mu_X \equiv \left(\mu_X^{331} - 1\right) \times 100\%$. We also introduce a new quantity $R_{Z\gamma/\gamma\gamma} \equiv |\delta\mu_{Z\gamma}/\delta\mu_{\gamma\gamma}|$ to investigate the relative difference between the two signal strengths. The recent allowed values relating with the two photon decay is $-15\% \leq \delta\mu_{\gamma\gamma} \leq 13\%$, the future sensitivities obtained by experiments we accept here are $\mu_{\gamma\gamma} = 1 \pm 0.04$ and $\mu_{Z\gamma} = 1 \pm 0.23$, i.e., $|\delta\mu_{\gamma\gamma}| \leq 4\%$ and $|\delta\mu_{Z\gamma}| \leq 23\%$, respectively.

Many well-known quantities used in this section are: $m_h = 125.09$ GeV; $m_W$, $m_Z$; the charged fermion masses; $v \simeq 246$ GeV, $g \simeq 0.651$, $\alpha_{\rm em} = 1/137$, $e = \sqrt{4\pi\alpha_{\rm em}}$, $s_W^2 = 0.231$.

The unknown independent parameters used as inputs are: $\beta$, $t_{12}$, $v_3$, $s_\delta$, $m_{h_2^0}$, $m_{h_3^0}$, $\lambda_1$, $\tilde{\lambda}_{12}$, $\tilde{\lambda}_{13}$, $\tilde{\lambda}_{23}$, $m_{E_a}$, $m_{J_a}$. We can put $m_{E_a} = m_{J_a} = m_F$ for simplicity. Accordingly at LHC, $m_{Z'} \geq 4$ TeV for 3-3-1 model with $\beta = -1/\sqrt{3}$ . Because $v_3 \sim \mathcal{O}(1)$ TeV, the $m_{Z'}$ is approximately caculated from $m_{Z'}^2 = \frac{g^2 v_3^2 c_W^2}{3[1-(1+\beta^2)s_W^2]}$. From this, $m_{Z'} > 4$ TeV corresponds to lower bounds of $v_3 \geq 10.6$, 10.1, 8.2, 3.3 TeV with respective values of $\beta = 0, \pm 1/\sqrt{3}, \pm 2/\sqrt{3}, \pm\sqrt{3}$. Recent discussion, $m_{Z'} = 3$ TeV or $v_3 \geq 7.6$ TeV for the 3-3-1 models with $\beta = -1/\sqrt{3}$ is allowed. On the other hand, a model with $\beta = \sqrt{3}$ still allows rather low $SU(3)_L$ scale, $m_{Z'} \simeq 3.25$ TeV, corresponding to $v_3 \simeq 2.7$ TeV. We will fixed $v = 14$ TeV for $|\beta| < \sqrt{3}$ and $v = 3$ TeV for $|\beta| = \sqrt{3}$.

The perturbative limits require that the absolute values of all Yukawa and Higgs self

couplings should be less than $\sqrt{4\pi}$ and $4\pi$, respectively. The result is $t_{12} < \sqrt{2\pi}v/m_t \simeq 3.5$. We will limit that $0.1 \leq t_{12} \leq 3$, which allows large $|s_\theta| \geq 5 \times 10^{-3}$. The values of $m_{h_2^0}$ and $m_{H^\pm}$ will be chosen to satisfy $m_{h_2^0}, m_{H^\pm} \geq 300$ GeV.

The Higgs potential is forced to satisfy the vacuum stability condition for the 3-3-1$\beta$ model, namely

$$\lambda_i > 0, \quad f_{ij} \equiv \lambda_{ij} + 2\sqrt{\lambda_i \lambda_j} > 0, \; \tilde{f}_{ij} \equiv \lambda_{ij} + \tilde{\lambda}_{ij} + 2\sqrt{\lambda_i \lambda_j} > 0, \tag{5.1}$$

where $i, j = 1, 2, 3$ and $i < j$.

The above discussion allows us to choose the default values of unknown independent parameters as follows: $\beta = 1/\sqrt{3}$, $s_\delta = 0.01$, $\lambda_1 = 1$, $t_{12} = 0.8$, $\tilde{\lambda}_{12} = \tilde{\lambda}_{13} = \tilde{\lambda}_{23} = 0.1$, $m_{h_2^0} = 1.2$ TeV, $m_{h_3^0} = 1$ TeV, $v_3 = 14$ TeV, $m_{E_a} = m_{J_a} = 1.5$ TeV. We choose the perturbative limit of Higgs self couplings is 10. In addition, depending on the particular discussions, changing any numerical values will be noted.

## 5.2 Numerical discussions

### 5.2.1 Case 1: $\tilde{\lambda}_{12} \geq 0$

First, we focus on the 2HDM parameters. Fig. 5.1 and 5.2 illustrate numerically Higgs-self couplings and $f_{ij}$ as functions of $m_{h_2^0}$, and other independent parameters are fixed as $t_{12} = 0.8$ and changing $s_\delta = \pm 10^{-2}, \pm 5 \times 10^{-2}$

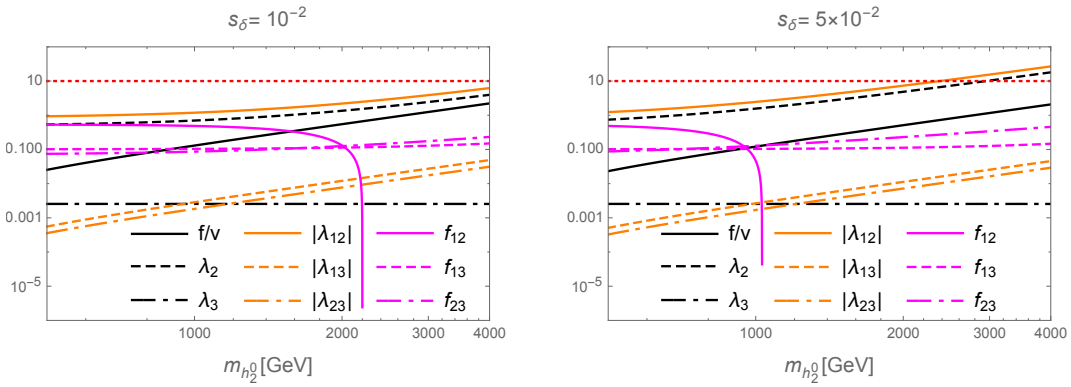


Figure 5.1: $f_{ij}$ and Higgs-self couplings as functions of $m_{h_2^0}$ with $s_\delta > 0$ and $t_{12} = 0.8$. The horizontal lines at the value of 10 correspond to the perturbative limit of the Higgs self couplings.

For $s_\delta > 0$, the $t_{12}$ is chosen large enough to satisfy $f_{12} > 0$ and $m_{h_2^0} > 1$ TeV. We conclude that the vacuum stability requirement $f_{12} > 0$ gives strong upper bound on $m_{h_2^0}$, where larger $s_\delta$ gives smaller allowed $m_{h_2^0}$. Fig. 5.2 illustrates allowed regions for $s_\delta < 0$, where we choose $t_{12} = 0.1$, enough small to allow $\lambda_2 > 0$ and $m_{h_2^0} > 1$ TeV. In general, our scan shows that allowed $t_{12}$ and $s_\theta$ are affected the most strongly by $m_{h_2^0}$. Fig. 5.3 presents allowed regions of $t_{12}$ and $s_\theta$ with two fixed $m_{h_2^0} = 1$ TeV and 2.5 TeV. It can be seen that larger $m_{h_2^0}$ results in smaller allowed $|s_\theta|$. The dashed black

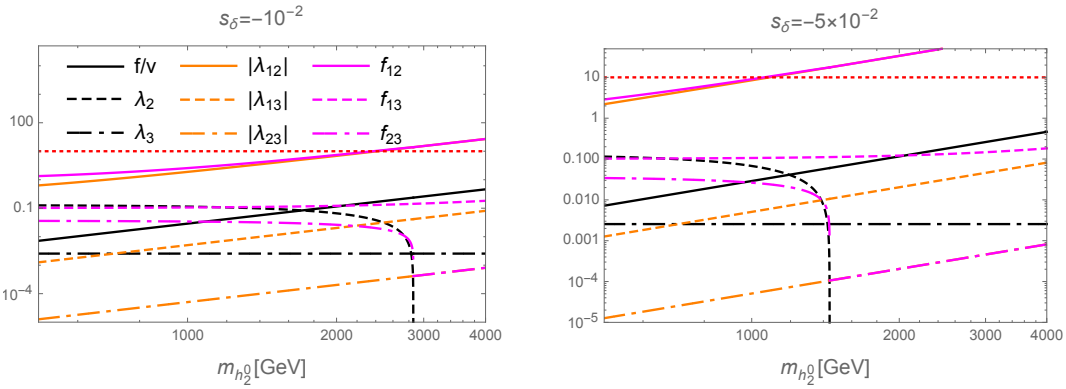


Figure 5.2: $f_{ij}$ and Higgs self couplings as functions of $m_{h_2^0}$ with $s_\delta < 0$ and $t_{12} = 0.1$.

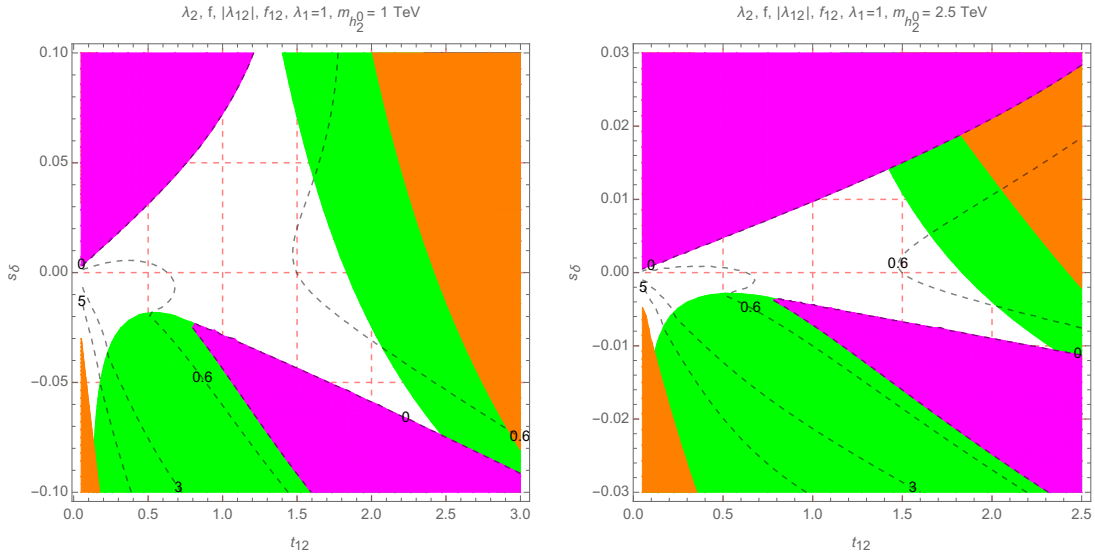


Figure 5.3: Contour plots of $\lambda_2$, $f$, $|\lambda_{12}|$ and $f_{12}$ as functions of $s_\theta$ and $t_{12}$. The green, blue, orange, magenta regions are excluded by requirements that $0 < \lambda_2 < 10$, $f > 0$, $|\lambda_{12}| < 10$, and $f_{12} > 0$, respectively. Dashed-black curves present constant values of $f_{12}$.

curves presenting constant values of $f_{12}$ will be helpful for the discussion on the case of $\tilde{\lambda}_{12} < 0$.

The allowed regions also depend on $\lambda_1$. It can be seen that $\lambda_1$ should be large enough to allow large $|s_\theta|$. In the case of large $|s_\theta| = 0.02$, the allowed values $\lambda_1$ and $t_{12}$ are shown in Fig. 5.4. It can be seen that only negative $s_\theta$ allows large $f_{12}$. The case of larger $|s_\theta| = 0.05$, we can choose $m_{h_2^0} = 1.2$ TeV so that $|s_\theta| = 0.05$ is still allowed. Both large $|s_\delta|$ and $m_{h_2^0}$ give narrow allowed regions of $t_{12}$ and $\lambda_1$, and small $f_{12}$. For small $|s_\delta| < 10^{-2}$, the allowed values of $m_{h_2^0}$ and $t_{12}$ will relax. But it will not result in much deviation from the SM prediction.

The left panel of Fig. 5.5 illustrates the contour plots with fixed $\beta = -1/\sqrt{3}$ for allowed values of $\delta\mu_{Z\gamma}$ corresponding to the none-color regions that satisfy the constraints of parameters and the recent experimental bound on $\delta\mu_{\gamma\gamma}$. The right panel

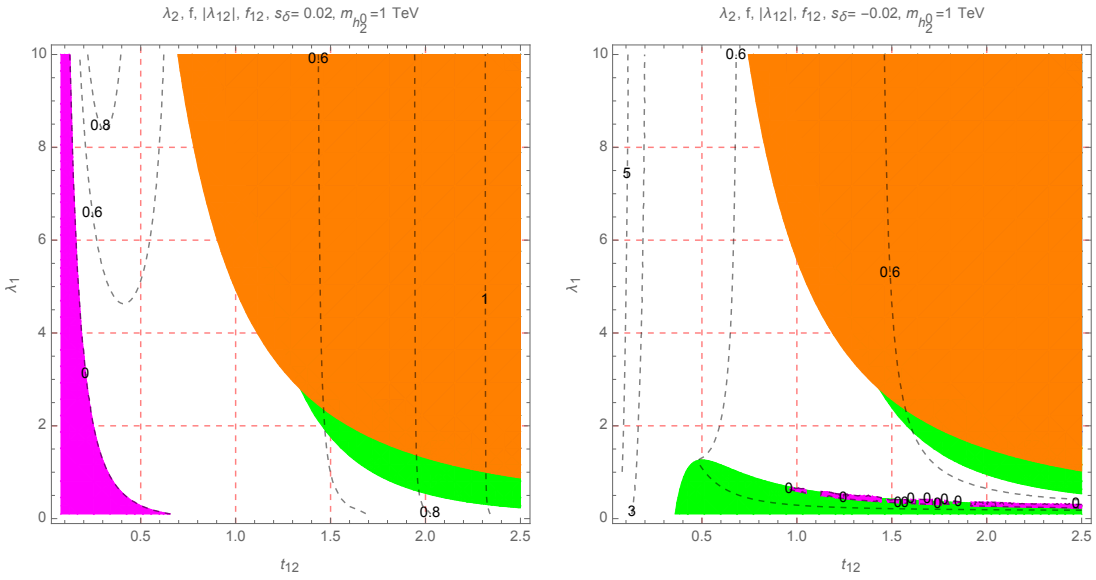


Figure 5.4: Contour plots of $\lambda_2$, $|\lambda_{12}|$ and $f_{12}$ as functions of $\lambda_1$ and $t_{12}$ with some fixed $m_{h_2^0}$ . The green, blue, orange, magenta regions are excluded by requirements that $0 < \lambda_2 < 10$, $f > 0$, $|\lambda_{12}| < 10$, and $f_{12} > 0$, respectively. Dashed-black curves present constant values of $f_{12}$.

of Fig. 5.5 shows the contour plots of $R_{Z\gamma/\gamma\gamma}$, where the non color region satisfies $R_{Z\gamma/\gamma\gamma} \geq 2$. In this region, we can see that $|s_\delta| \sim \mathcal{O}(10^{-3})$ and negative. In addition, $\delta\mu_{\gamma\gamma} < 0.04$. Hence, the current constraints $\mu_{\gamma\gamma} = 0.99 \pm 0.14$ predicts $|\delta\mu_{Z\gamma}| < 0.15$ which is still smaller than the future sensitivity $\delta\mu_{Z\gamma} = \pm 0.23$. In addition, most of the allowed regions satisfies $0.8 \leq R_{Z\gamma/\gamma\gamma} \leq 2$, hence the approximation $\text{Br}(h \to \gamma\gamma) \simeq \text{Br}(h \to Z\gamma)$ is accepted for simplicity in previous works.

For large $v_3 = 14$ TeV and recent uncertainty of the $\delta\mu_{\gamma\gamma}$, our investigation shows generally that the above discussions on the allowed regions as well as $R_{Z\gamma/\gamma\gamma}$ illustrated in Fig. 5.5 depend weakly on $\beta$. The results are also unchanged for lower bound of $v_3 = 8$ TeV which is allowed for $\beta = \pm 2/\sqrt{3}$. This property can be explained by the fact that, large $v_3 \simeq 10$ TeV results in heavy charged gauge bosons $m_Y, m_V \geq 4$TeV, and the charged Higgs masses being not less than 1 TeV. As a by product, one loop contributions from $SU(3)_L$ particles to $F_{21}^{331}$ and $F_{\gamma\gamma}^{331}$ are at least four orders smaller than the corresponding SM amplitudes $F_{21,\gamma\gamma}^{\text{SM}}$, illustrations are given in table 5.1. Here

| $\beta$ | $s_\delta$ | $t_{12}$ | $\frac{F_{21,s}^{331}}{\text{Re}[F_{21}^{\text{SM}}]}$ | $\frac{F_{21,v}^{331}}{\text{Re}[F_{21}^{\text{SM}}]}$ | $\frac{F_{21,sv}^{331}}{\text{Re}[F_{21}^{\text{SM}}]}$ | $\frac{F_{\gamma\gamma,s}^{331}}{\text{Re}[F_{\gamma\gamma}^{\text{SM}}]}$ | $\frac{F_{\gamma\gamma,v}^{331}}{\text{Re}[F_{\gamma\gamma}^{\text{SM}}]}$ | $\delta\mu_{Z\gamma}$ | $\delta\mu_{\gamma\gamma}$ |
|---|---|---|---|---|---|---|---|---|---|
| $\frac{2}{\sqrt{3}}$ | $2 \times 10^{-2}$ | 1.5 | $-3.3 \times 10^{-4}$ | $3 \times 10^{-5}$ | $-1.6 \times 10^{-4}$ | $-6 \times 10^{-4}$ | $5.5 \times 10^{-4}$ | 4.4 | 6.5 |
| $\frac{2}{\sqrt{3}}$ | $-2 \times 10^{-2}$ | 1.5 | $\sim 10^{-6}$ | $3 \times 10^{-5}$ | $-1.5 \times 10^{-4}$ | $\sim 10^{-6}$ | $5.3 \times 10^{-4}$ | $-5.4$ | $-6$ |
| $\frac{2}{\sqrt{3}}$ | $2 \times 10^{-2}$ | 0.5 | $1.3 \times 10^{-4}$ | $-9 \times 10^{-5}$ | $-5 \times 10^{-5}$ | $2.3 \times 10^{-4}$ | $2.2 \times 10^{-4}$ | 6.8 | 8.1 |
| $\frac{2}{\sqrt{3}}$ | $-2 \times 10^{-2}$ | 0.5 | $-4.2 \times 10^{-4}$ | $-9 \times 10^{-5}$ | $-4 \times 10^{-5}$ | $-7.5 \times 10^{-4}$ | $2.1 \times 10^{-4}$ | $-7.5$ | $-7.4$ |
| $\frac{2}{\sqrt{3}}$ | $-10^{-3}$ | 1.5 | $-1.6 \times 10^{-4}$ | $3 \times 10^{-5}$ | $-1.6 \times 10^{-4}$ | $-2.9 \times 10^{-4}$ | $5.4 \times 10^{-4}$ | $-0.8$ | $-0.2$ |

Table 5.1: Numerical contributions of $SU(3)_L$ particles to $F_{21}^{331}$ and $F_{\gamma\gamma}^{331}$, where $F_{21,sv}^{331} \equiv F_{21,svv}^{331} + F_{21,vss}^{331}$.

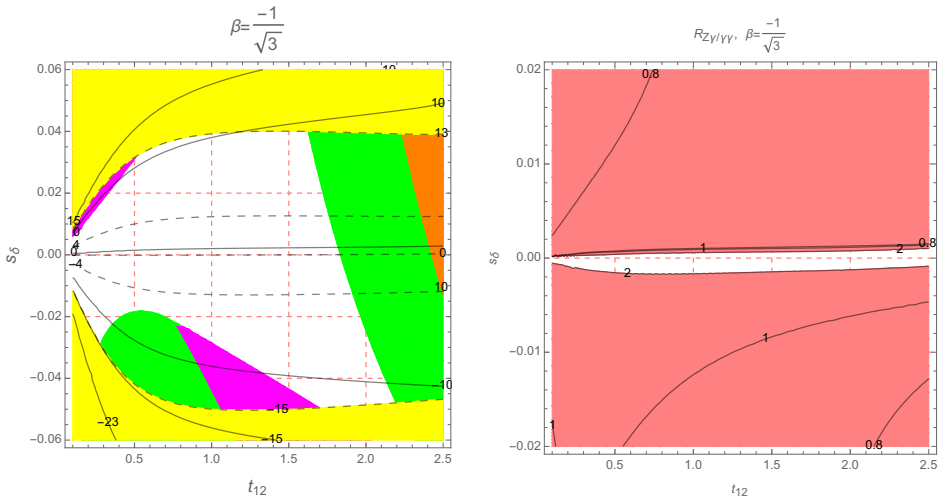


Figure 5.5: Contour plots showing allowed regions of $s_\delta$ and $t_{12}$ (left) and $R_{Z\gamma/\gamma\gamma}$ as a function of $s_\delta$ and $t_{12}$. The green, blue, orange, magenta and yellow regions are excluded by valid requirements of $\lambda_2, f, \lambda_{12}, f_{12}$, and $\delta\mu_{\gamma\gamma}$, respectively. The black and dotted black curves show constant values of $\delta\mu_{Z\gamma}$ and $\delta\mu_{\gamma\gamma}$, respectively. The non color region in the right panel corresponds to $R_{Z\gamma/\gamma\gamma} \geq 2$.

we use the SM amplitudes $\text{Re}[F_{21}^{\text{SM}}] = -5.6 \times 10^{-5}\,[\text{GeV}^{-1}]$ and $\text{Re}[F_{\gamma\gamma}^{\text{SM}}] = -3.09 \times 10^{-5}\,[\text{GeV}^{-1}]$. We note that $F_{21,sv}^{331}$ may be significantly larger than $F_{21,v}^{331}$, hence both of them should be included simultaneously into the decay amplitude $h \to Z\gamma$ in general.

For large and positive $\tilde{\lambda}_{12}$ and small $m_{h_2^0}$, one loop contributions from $H^\pm$ to $F_{21}^{331}$ and $F_{\gamma\gamma}^{331}$ are dominant but still not large enough to give significant deviations to $\delta\mu_{Z\gamma}$, see an illustration with suppressed $s_\delta = 10^{-3}$ in the first line of table 5.2. Here we

| $\beta$ | $s_\delta$ | $t_{12}$ | $\frac{F_{21,s}^{331}}{\text{Re}[F_{21}^{\text{SM}}]}$ | $\frac{F_{21,v}^{331}}{\text{Re}[F_{21}^{\text{SM}}]}$ | $\frac{F_{21,sv}^{331}}{\text{Re}[F_{21}^{\text{SM}}]}$ | $\frac{F_{\gamma\gamma,s}^{331}}{\text{Re}[F_{\gamma\gamma}^{\text{SM}}]}$ | $\frac{F_{\gamma\gamma,v}^{331}}{\text{Re}[F_{\gamma\gamma}^{\text{SM}}]}$ | $\delta\mu_{Z\gamma}$ | $\delta\mu_{\gamma\gamma}$ |
|---|---|---|---|---|---|---|---|---|---|
| $\frac{2}{\sqrt{3}}$ | $10^{-3}$ | 1.7 | $-1.46 \times 10^{-2}$ | $4 \times 10^{-5}$ | $-1.7 \times 10^{-4}$ | $-2.64 \times 10^{-2}$ | $5.7 \times 10^{-4}$ | $-3.1$ | $-4.7$ |
| $\frac{2}{\sqrt{3}}$ | $-10^{-3}$ | 1.7 | $-1.44 \times 10^{-2}$ | $4 \times 10^{-5}$ | $-1.7 \times 10^{-4}$ | $-2.61 \times 10^{-2}$ | $5.7 \times 10^{-4}$ | $-3.6$ | $-5.3$ |
| $\frac{2}{\sqrt{3}}$ | $3 \times 10^{-2}$ | 1.5 | $-1.24 \times 10^{-2}$ | $3 \times 10^{-5}$ | $-1.6 \times 10^{-4}$ | $-2.23 \times 10^{-2}$ | $5.5 \times 10^{-4}$ | 4.4 | 5.2 |
| $\frac{2}{\sqrt{3}}$ | $-3 \times 10^{-2}$ | 1.5 | $-9.6 \times 10^{-3}$ | $3 \times 10^{-5}$ | $-1.5 \times 10^{-4}$ | $-1.75 \times 10^{-3}$ | $5.3 \times 10^{-4}$ | $-9.6$ | $-12.3$ |

Table 5.2: Numerical contributions of $SU(3)_L$ particles to $F_{21}^{331}$ and $F_{\gamma\gamma}^{331}$ for large $\tilde{\lambda}_{12} = 5$ and small $m_{h_2^0} = 600$ GeV.

always force $|\delta\mu_{\gamma\gamma}| \leq 4\%$ being the future sensitive of $\mu_{\gamma\gamma}$.

Regarding $\beta = \sqrt{3}$, where $v_3 = 3$ TeV is still accepted, the allowed regions change significantly, as illustrated in Fig. 5.6. In particularly, the model gives more strict positive $s_\delta < 0.03$. One-loop contributions from $SU(3)_L$ particles can give deviations up to few percent for both $\delta\mu_{Z\gamma}$, $\delta\mu_{\gamma\gamma}$, while two contours $\delta_{Z\gamma} = \delta\mu_{\gamma\gamma} = 0$ distinguish with the line $s_\delta = 0$. Interesting numerical values are illustrated in Table 5.3.

We emphasize two important properties. First, one loop contributions from gauge $SU(3)_L$ bosons are dominant, which can give $\delta\mu_{\gamma\gamma}$ to reach the future sensitivity. Second, values of $F_{21,v}^{331}$ and $F_{21,sv}^{331}$ can have the same order of $10^{-3}$ compared with the

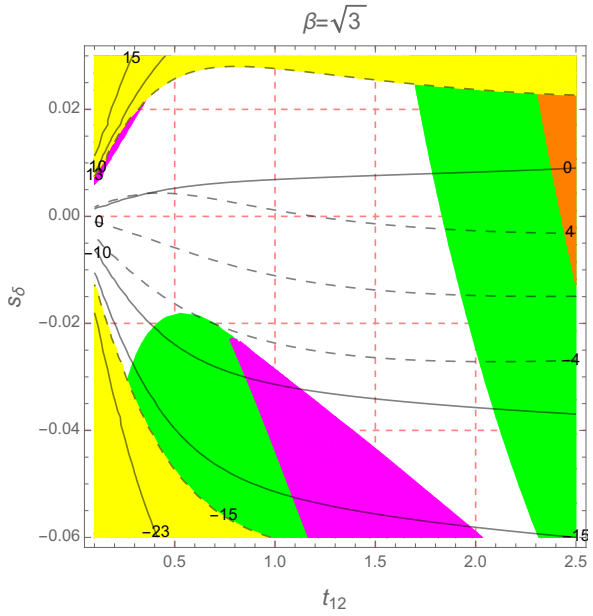


Figure 5.6: Contour plots showing allowed regions of $s_\delta$ and $t_{12}$ with $v_3 = 3$ TeV. The green, blue, orange, magenta and yellow regions are excluded by valid requirements of $\lambda_2, f, \lambda_{12}, f_{12}$, and $\delta\mu_{\gamma\gamma}$, respectively. The black and dotted black curves show constant values of $\delta\mu_{Z\gamma}$ and $\delta\mu_{\gamma\gamma}$, respectively.

| $\beta$ | $s_\delta$ | $t_{12}$ | $\frac{F^{331}_{21,s}}{\mathrm{Re}[F^{\mathrm{SM}}_{21}]}$ | $\frac{F^{331}_{21,v}}{\mathrm{Re}[F^{\mathrm{SM}}_{21}]}$ | $\frac{F^{331}_{21,sv}}{\mathrm{Re}[F^{\mathrm{SM}}_{21}]}$ | $\frac{F^{331}_{\gamma\gamma,s}}{\mathrm{Re}[F^{\mathrm{SM}}_{\gamma\gamma}]}$ | $\frac{F^{331}_{\gamma\gamma,v}}{\mathrm{Re}[F^{\mathrm{SM}}_{\gamma\gamma}]}$ | $\delta\mu_{Z\gamma}$ | $\delta\mu_{\gamma\gamma}$ |
|---|---|---|---|---|---|---|---|---|---|
| $\sqrt{3}$ | $10^{-3}$ | 1.5 | $-1.8\times10^{-4}$ | $-1.6\times10^{-3}$ | $-4\times10^{-3}$ | $-3.2\times10^{-4}$ | $2.2\times10^{-2}$ | $-1.6$ | 4.8 |
| $\sqrt{3}$ | $-10^{-3}$ | 1.5 | $-1.6\times10^{-4}$ | $-1.7\times10^{-3}$ | $-4\times10^{-3}$ | $-2.9\times10^{-4}$ | $2.2\times10^{-2}$ | $-2$ | 4.2 |

Table 5.3: Numerical contributions of $SU(3)_L$ particles to $F^{331}_{21}$ and $F^{331}_{\gamma\gamma}$. Notations are given from caption of table 5.1.

SM part, but they are not large enough to result in large deviation of $|\delta\mu_{Z\gamma}| > 23\%$.

We stress here an interesting point that with the existence of new Higgs and gauge bosons, their contributions $F^{331}_{\gamma\gamma,s}$ and $F^{331}_{\gamma\gamma,v}$ to the decay amplitude $h \to \gamma\gamma$ may be destructive and the same order, hence keep the respective signal strength satisfying the small experimental constraint. Simultaneously, all of the contributions to the decay amplitude $h \to Z\gamma$ are constructive so that the deviation can be large. For the model with $\beta = \sqrt{3}$ and $v_3 = 3$ TeV, we can find this deviation can reach around $-10$, but this values is still far from the expected sensitive $\delta\mu_{Z\gamma} = \pm 23\%$. For the models with $v_3 \geq 8$ TeV, heavy gauge contributions are suppressed, hence large contribution from charged Higgs bosons is dominant. Then, the constraint from $\delta\mu_{\gamma\gamma}$ will give more strict constraint on $\delta\mu_{Z\gamma}$ than that obtained from the experiments.

### 5.2.2 Case 2: $\tilde{\lambda}_{12} < 0$.

With $\tilde{\lambda}_{12} < 0$, constructive contributions appear in the decay amplitude $h \to \gamma\gamma$, while destructive contributions appear in the decay amplitude $h \to Z\gamma$. Hence, the

constraint from experimental data of the decay $h \to \gamma\gamma$ predicts smaller deviation of the $\mu_{Z\gamma}$ than that corresponding to $\tilde{\lambda}_{12} > 0$.

### 5.2.3 $h_3^0$ decays as a signal of the $3-3-1\beta$ model

Different contributions to loop-induced decays $h_3^0 \to \gamma\gamma, Z\gamma$ with small $s_\theta = 10^{-3}$, $m_{h_3^0} = 700$ GeV, $t_{12} = 0.8$ are illustrated in Fig. 5.7, where the ratios $|F_{21,x}(h_3^0 \to Z\gamma)|/|F_{21}(h_3^0 \to Z\gamma)|$ and $|F_{\gamma\gamma,x}(h_3^0 \to Z\gamma)|/|F_{\gamma\gamma}(h_3^0 \to Z\gamma)|$ are presented, $x = f, s, v, sv$. The contributions from heavy exotic fermions are alway dominant for large $\beta$. While

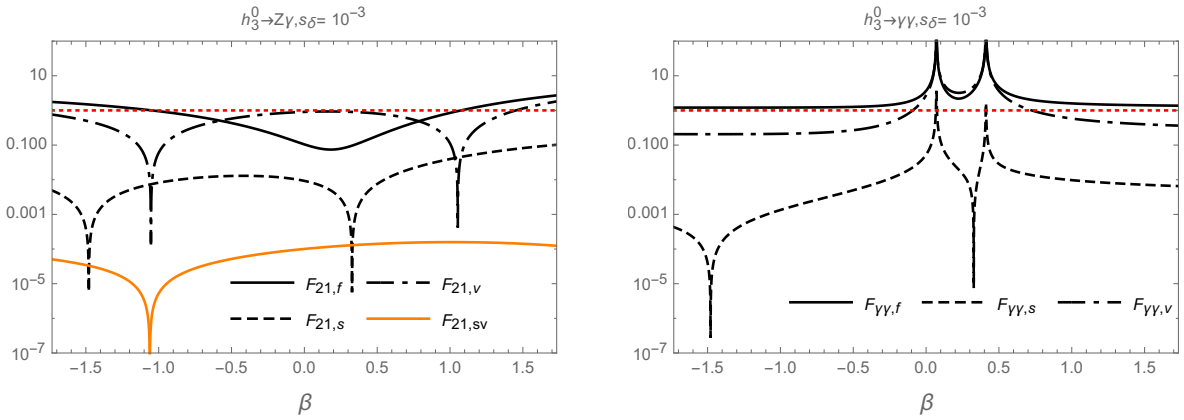


Figure 5.7: Different contributions to loop-induced decays $h_3^0 \to \gamma\gamma, Z\gamma$ as functions of $\beta$.

$F_{21,sv}$ is suppressed. For the decay $h_3^0 \to \gamma\gamma$, the destructive correlation between $F_{\gamma\gamma,v}$ and $F_{\gamma\gamma,f}$ happens with small $|\beta|$.

Individual branching ratios of $h_3^0$ are shown in Fig. 5.8. The most interesting prop-

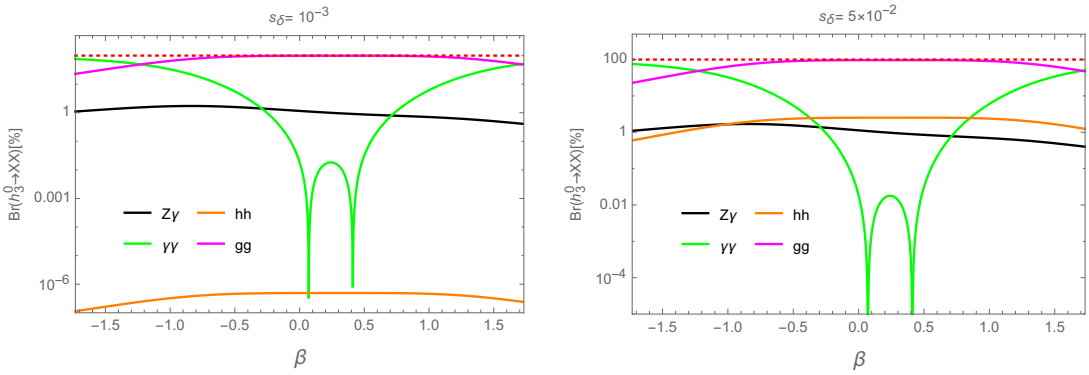


Figure 5.8: Branhching ratios of the $h_3^0$ decays as functions of $\beta$.

erty is that, the $\mathrm{BR}(h_3^0 \to \gamma\gamma)$ may have large values and it is very sensitive with the change of $\beta$. Hence this decay is a promising channel to fix the $\beta$ value once $h_3^0$ exists. On the other hand, $\mathrm{BR}(h_3^0 \to hh)$ is sensitive with $s_\delta$: it increases significantly with large $s_\delta$, but the values is always small $\mathrm{BR}(h_3^0 \to hh) < 1\%$.

# CONCLUSIONS

Investigating the two SM-like Higgs boson decays $h \to Z\gamma$ in the 3-3-1$\beta$ model and $h \to \mu\tau$ in the flipped 3-3-1 model, we obtain the following new results:

- In the flipped 3-3-1 model:

  + We have established the analytic formulas expressing one-loop contributions to the branching ratio of the decays $h \to \mu\tau, \mu \to e\gamma$.

  + Determining allowed regions of the parameter space that satisfy the experimental bound on cLFV. At the same time, the LFVHD branching ratio is large enough for experiments to be measured. Investigating the dependencies of Br($h \to \mu\tau, \mu \to e\gamma$) on the parameters $(M_E)$, $(s_{ij})$, $(k_1)$, new results are:

  - The main LFV sources originate from the heavy charged leptons. One loop contributions to the LFV decay amplitudes $h \to \mu\tau$ and $\tau \to \mu\gamma$ are larger than those of $h \to \tau e, \mu e$ and $\tau, \mu \to e\gamma$, respectively.

  - Br($h \to \tau\mu, \tau e$) and Br($h \to \mu e$) can reach the order $\mathcal{O}(10^{-3}-10^{-4})$ and $\mathcal{O}(10^{-6})$ respectively, very close to the recent experimental lower bounds. They should be used for constraining the parameter space for future improved lower bounds.

  - BR($\tau \to \mu\gamma, e\gamma$) $\leq \mathcal{O}(10^{-14})$, much smaller than the planed sensitivities of upcoming experiments. BR($\mu \to e\gamma$) can reach the order of $\mathcal{O}(10^{-15})$ which is more promising for searching by experiments.

- In the 3-3-1$\beta$ model:

  + One-loop contribution on BR($h \to Z\gamma, \gamma\gamma$). They depend weakly on $\beta$. $F^{331}_{21,sv}$ and $F^{331}_{21,v}$ can have the same order. Hence, $F^{331}_{21,sv}$ should not be ignored. For $\beta = \sqrt{3}$, gauge and Higgs contributions may be large and have the same order.

  + There may exist recent gauge extensions of the BSM that allow large $|\delta\mu_{Z\gamma}|$, while still satisfy the future experimental constraint $|\delta\mu_{\gamma\gamma}| \leq 0.04$.

  + Our numerical investigation obtains: (i) The large deviations $\delta\mu_{Z\gamma}$ originate from the one-loop contribution of $H^{\pm}$ and large $|s_\delta|$, and $|\delta\mu_{Z\gamma}| \leq |\delta\mu_{\gamma\gamma}| < 0.23$ for large $v_\chi \geq 14$ TeV. In the 3-3-1 with $\beta = \sqrt{3}$ and $v_3 \simeq 3$ TeV, $\delta\mu_{Z\gamma}$ may be large in the allowed region $\mu_{\gamma\gamma} = 0.99 \pm 0.14$. For the near future sensitivity $|\delta\mu_{\gamma\gamma}| = 0.04$, this model still allows $|\delta\mu_{Z\gamma}| \leq 0.1$, but it canot reach the near future sensitivity $|\delta\mu_{Z\gamma}| = 0.23$.

  - The total decay width of the $h^0_3$ and $BR(h^0_3 \to \gamma\gamma, Z\gamma)$ are an important signal to distinguish different 3-3-1 models.

## LIST OF PUBLICATIONS RELATED TO THESIS

1. H. T. Hung, T. T. Hong, **H. H. Phuong**, H. L. T. Mai and L. T. Hue, "*Neutral Higgs decays $H \to Z\gamma, \gamma\gamma$ in 3-3-1 models*", Phys. Rev. D **100**, 075014 (2019).

2. T. T. Hong, H. T. Hung, **H. H. Phuong**, L. T. T. Phuong and L. T. Hue, "*Lepton-flavor-violating decays of the SM-like boson Higgs $h \to e_i e_j$, and $e_i \to e_j\gamma$ in a flipped 3-3-1 model*", PTEP **2020**, 043B03 (2020).